Electron energy loss spectroscopy and *ab initio* investigation of iron oxide nanomaterials grown by a hydrothermal process

Shih-Yun Chen,[1,2,*] Alexandre Gloter,[2,†] Alberto Zobelli,[2] Leeyih Wang,[3] Cheng-Hsuan Chen,[3] and Christian Colliex[2]
[1]*Department of Polymer Engineering, National Taiwan University of Science and Technology, Taipei, Taiwan*
[2]*Laboratoire de Physique des Solides, CNRS-UMR 8502, Université Paris Sud, 91405 Orsay, France*
[3]*Center for Condensed Matter Sciences, National Taiwan University, Taipei, Taiwan*
(Received 14 October 2008; published 5 March 2009)

We first describe with the help of reference experiments (at the Fe 2*p* and O 1*s* edges) and *ab initio* calculations how electron energy loss spectroscopy (EELS) can be used in order to characterize phases of iron oxide and/or hydroxide nanomaterials. In particular we show that dehydration of iron hydroxides such as goethite can easily appear under the electron beam but might be followed by monitoring the O *K* peak. Indeed both local spin-density approximation (LSDA) and LSDA+*U* calculations confirm that intensity of the prepeak of O *K* should increase while H atoms are removed. We also demonstrate that different magnetic orders do not change significantly the O *K* EELS fine structure of goethite. Thus, nanomaterials (particles and wires) synthesized by a hydrothermal treatment of nanoscale (10–40 nm) magnetite particles have been conducted. Among them, crystalline iron oxide nanowires with average diameter of 20 nm and length of up to 10 μm are reported. The O *K* edge and Fe $L_{2,3}$ edges were studied by EELS for these nanostructures. The results indicated that the valence of iron is 3+ in the wires while it is the mixture of 2+ and 3+ in the particles. From these combined EELS, scanning transmission electron microscopy, diffraction, and high-resolution electron microscopy, the complexity of the produced phases from these hydrothermal treatments can be revealed. This work shows how EELS with high-energy resolution is a unique tool to differentiate iron oxide compounds such as the tricky magnetite-maghemite solid solution or the case of partially dehydrated phases, even on a nanometer scale.

DOI: 10.1103/PhysRevB.79.104103 PACS number(s): 68.49.Uv, 31.15.ae, 31.15.es, 61.46.Km

I. INTRODUCTION

Complex oxides with a tremendous variety in crystal structures play an essential role in modern science and technology. By selecting appropriate constituent elements, the associated crystals and derived electronic structures of oxides can be altered by manipulating the delicate equilibrium in the bonding requirements of a lattice, thus leading to a wide spectrum of physical properties, e.g., magnetism and superconductivity. Notably, the physical properties in bulks can change as the size of materials shrinks. Considering the growing interests in reducing material size for applications, it is crucial to examine the potential impact of dimensionality on the physical properties of finite complex oxides.

Among these, the electronic structure of iron oxides has been the subject of many experimental and theoretical studies. In particular, in the case of Fe_3O_4 (magnetite), the high phase-transition temperature (858 K) and the atmospheric stability render this compound an extraordinarily promising material for magnetic recording media. It is ferrites with inverse spinel structure, whereby the oxygen ions form a fcc lattice and the iron ions occupy tetrahedral and octahedral sites.

Recent approaches in nanosciences further suggest that Fe_3O_4 nanowires (NWs) can be integrated into magnetic memory storage arrays. The preparation of NWs with single magnetite phase, which ensures structural uniformity, thus becomes increasingly important. The synthesis of magnetite is delicate,[1–3] which is sensitive to temperature, pH values, applied magnetic field, reaction time, and so on. On the other hand, according to chemical thermodynamics, Fe_3O_4, γ-Fe_2O_3 (maghemite), α-Fe_2O_3 (hematite), and α-FeOOH (goethite) are easy to be found simultaneously in iron oxide system. Goethite is the most common and most stable natural Fe-oxyhydroxide, and hematite is the most stable iron oxide compound. In addition, it is difficult to distinguish Fe_3O_4 and γ-Fe_2O_3 on nanometer scale because of their structural similarities.[4]

In recent years, EELS has been demonstrated to be a useful tool to study electronic structure of materials. In the past, the variations in oxidation state of transition metals were examined according to the change in white line intensity ratio, L_3/L_2. It varies with *d*-band occupancy across the periodic table and the charge state of the metal atom.[5] The exact cause of this anomalous behavior is due to a number of effects and has been studied by many authors.[6,7] Nowadays, with the improvement of energy resolution, by either hardware or software, near-edge fine structures [energy loss near-edge structure (ELNES)] of spectra can be obtained. ELNES provides much more information about bonding, site symmetry, and oxidation state.

In this paper, we demonstrate that high-energy resolved electron energy loss spectroscopy (EELS) can be used at the nanometer scale in iron oxide and iron hydroxide systems. In Sec. III, we will briefly summarize the expected fine structures of Fe *L* and O *K* edges from reported x-ray absorption spectroscopy (XAS) and EELS for various iron oxides and present some Fe *L* and O *K* edges obtained by our spectroscopic system. We also point out that iron hydroxides may be easily transformed under the electron beam of the transmission electron microscope by showing the evolution of the O *K* edge of a goethite. In Sec. IV, the O *K* edges of hematite

and goethite have been computed utilizing *ab initio* method. The influence of the hydroxyl bonding in the prepeak shape of the O *K* edges of iron oxides is thus discussed. These results suggest that high-energy resolved EELS on O *K* edges can probe the local average connectivity of oxygen with iron and can be useful to distinguish between iron oxide and iron hydroxide on nanometer scale. In the Sec. V, a nanoscale Fe-O system obtained by hydrothermal process was analyzed by utilizing the above-mentioned ELNES and density-functional-theory (DFT)-based calculations. Up to four different phases among the iron-oxygen compounds are observed: some of the nanowires are maghemite (γ-Fe_2O_3) phase and others are goethite (α-FeOOH). The nanoparticles (NPs) observed in the product are magnetite (Fe_3O_4) with the surface altered during the hydrothermal process. After long reaction time, hematite (α-Fe_2O_3) in the form of large platelets was found.

II. EXPERIMENTAL SECTION

In this study, a field- and template-free hydrothermal synthesis of iron oxide NWs using seeding NPs was performed. Seeding NPs were first coprecipitated at room temperature from starting chemicals, $FeCl_2 \cdot 4H_2O$, $FeCl_3 \cdot 6H_2O$, and NH_4OH.[8,9] After careful washing and drying, these NPs were combined with NaOH solution (10 M) and sealed in a Teflon autoclave at 130 °C for 40 and 60 h, respectively, for hydrothermal synthesis of the NWs. Following the reaction, precipitates in the autoclave were filtered, washed, and dried at 50 °C.

Hematite and siderite reference samples are from mineralogical origin (respectively, from Ouro Preto mine, Brazil and Saint Georges d'Hurtière mine, France). Magnetite reference samples from two origins have been investigated and show no spectroscopic differences (biomineralized crystal from magnetotactic bacteria MV-1 and inorganic crystal from Aldrich-Ltd). Akageneite, goethite, and 2l-ferrihidrite have been synthesized by chemical routes.

The scanning transmission electron microscopy high-angle annular dark field (STEM-HAADF) and scanning transmission electron microscopy electron energy loss spectroscopy (STEM-EELS) measurements have been performed with a dedicated scanning transmission electron microscope (Vacuum Generators HB501) equipped with a home modified Gatan spectrometer. All spectra are recorded in STEM mode with 100 keV incident electrons focused on the specimen. The probe size is at around 0.8 nm and the current intensity varies from 100 to 300 pA depending on the tuning conditions of the emitting tip. Energy resolution of the cold field emitter is around 0.35 eV, when measured at the full width at half maximum (FWHM) of the zero-loss peak.

The high-resolution electron microscopy (HREM) and selected area electron diffraction (SAED) measurements have been realized on a transmission electron microscopy (TEM) JEOL 2010 equipped with an ultra high-resolution pole piece (spherical aberration coefficient Cs of 0.5 mm).

III. ELECTRON ENERGY LOSS SPECTRA AT THE Fe 2*p* AND O 1*s* EDGES OF IRON OXIDES AND HYDROXIDES

To compare EELS edges coming from different valence and environment, Fig. 1 shows Fe 2*p* edges of implicated

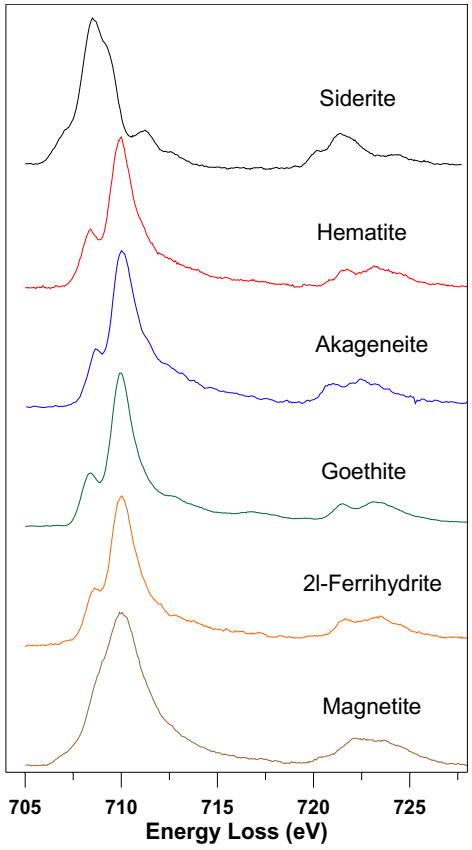

FIG. 1. (Color online) Fe *L* edges obtained from siderite ($FeCO_3$), hematite (α-Fe_2O_3), akageneite (β-FeOOH), goethite (α-FeOOH), 2*l*-Ferrihydrite (quoted HFO for hydrous ferric oxide), and magnetite (Fe_3O_4) by using our spectrometer. In order to observe the transitions to the Fe 3*d* states, the edge extraction has been done by constraining a zero value before the L_3 line and after the L_2 line. The contributions from the transitions to the continuum states are then not visible.

iron oxides obtained by using our spectroscopic equipment. Here we compare Fe 2*p* edges obtained from reference siderite ($FeCO_3$), hematite (α-Fe_2O_3), and magnetite (Fe_3O_4). Besides, iron hydroxide phases, 2*l*-Ferrihydrite (HFO), akageneite (β-FeOOH),[33] and goethite (α-FeOOH),[34] $L_{2,3}$ edges have also been reported. The O 1*s* are also gathered for the same phases in the Fig. 2. The experimental results are described below.

A. Experimental EELS Fe 2*p* edges

Over the past several decades, iron $L_{2,3}$ edges have been studied by EELS (Refs. 9–14) and XAS (Refs. 15 and 16) at different energy resolution, spatial resolution, and angular resolution in various contexts, such as mineralogy and environmental science.[17–19] For ferric and ferrous iron, Fe $L_{2,3}$ edges can be primary described as transitions from a ground state, Fe $2p^6 3d^5$ ($2p^6 3d^6$), to a final excited state, Fe $2p^5 3d^6$ ($2p^5 3d^7$), respectively. Calculated spectra based on the nearly atomic transition of these configurations have shown different fine structures for these two valence states.[20] It has also been reported that the position of L_3 maximum line

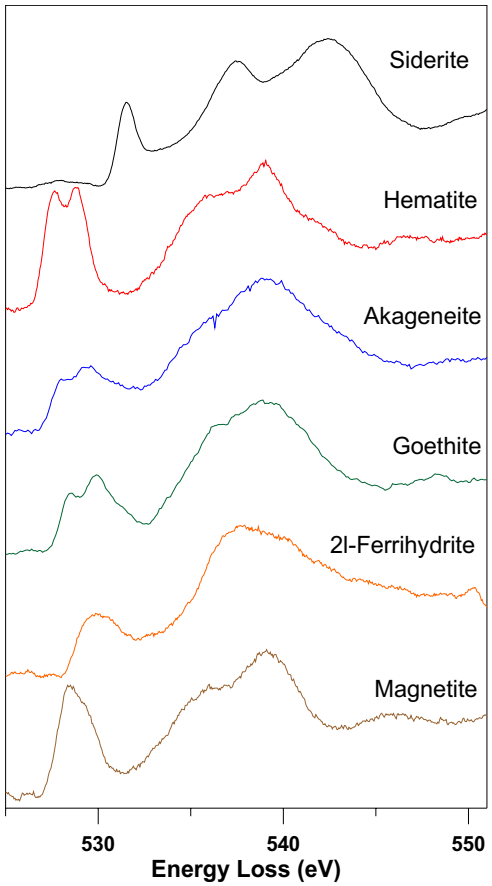

FIG. 2. (Color online) O K edges obtained from siderite ($FeCO_3$), hematite (α-Fe_2O_3), akageneite (β-FeOOH), goethite (α-FeOOH), 2l-Ferrihydrite (quoted HFO for hydrous ferric oxide), and magnetite (Fe_3O_4) by using our spectrometer.

changes as a function of the valence. This chemical shift was attributed to a change in the number of electron on the d band.[21] Based on these differences, several techniques have been reported for the iron valence quantification.[12,13] The accuracy of such determination is limited by the resolution and the experimental conditions.[11] Notably, the structure of the edges for a given valence may be altered by various solid-state effects.[22]

As the reported XAS (Refs. 16 and 20) and EELS (Refs. 23 and 24) results, Fe 2p edges in hematite show typical $L_{2,3}$ edges for trivalent iron with a strong prepeak at the L_3 edge. The prepeak is located around 1.6 eV in front of maximum of the L_3 line. This was partially attributed to the strong crystal-field splitting from octahedral symmetry around the iron site.

Siderite spectrum shows a chemical shift toward lower energy as expected for a divalent material with respect to the trivalent. The L_3 line shows a more complex splitting than that for the trivalent one. Similar fine structures have been reported for other divalent materials such as wustite FeO (Ref. 12) or Fayalite Fe_2SiO_4.[14] As showed by Garvie and Buseck,[12] most of the mixed-valence spectra may be hence decomposed as a linear combination of two reference spectra for divalent and trivalent iron.

On the other hand, magnetite is a mixed-valence compound and shows an unusual $L_{2,3}$ edges. L_2 edge shows a typical shape for a mixed-valence compound, i.e., three visible features of different intensities were observed. On the other hand, L_3 edge appears almost shapeless, even when collected a very high energy resolution by synchrotron radiation.[25–31] This has been interpreted as the result of the mixture of various iron sites[15] and of the more delocalized electronic structure of magnetite compared to most of other mixed iron oxides.[32]

As for iron hydroxide phases such as 2l-Ferrihydrite (HFO), akageneite (β-FeOOH),[33] and goethite (α-FeOOH),[34] $L_{2,3}$ edges have also been reported. All fine structures arise from Fe^{3+} ground state. Nevertheless, the splitting in prepeak of the iron hydroxide seems significantly smaller than that in hematite, indicating a weaker crystal field around the Fe atoms, especially when the crystallization is poor (2l-ferrihydrite for example).

In Fig. 1, we did not present $L_{2,3}$ edges of maghemite (γ-Fe_2O_3). However, it has been studied before. All the reported data show that Fe $L_{2,3}$ edge in maghemite is primary trivalent ground state and with a visible splitting in the L_3. However, inconsistent fine structures were reported[35–37] and this was attributed to the remnant ferric (Fe^{2+}) in material. Accordingly, the value of the splitting in L_3 for the pure spectrum of maghemite may be difficult to assess because of the quality of the sample. But it has been generally found that as comparing to that in hematite, the splitting in maghemite is smaller[31] (1.3 eV).

B. Experimental EELS O 1s edges

Generally, the reported O K edges of different iron oxides show a similar feature, i.e., it is composed of a prepeak and a broad edge at higher energy. The former results from the hybridization of Fe 3d and O 2p and it usually splits into t_{2g} and e_g states by the ligand field. The latter is composed of density of states (DOS) from oxygen p character hybridized with metal 4s and 4p states. This is a general description and it holds for most of the transition-metal oxides.[38] The intensity of the prepeak may change as a function of the oxygen connectivity and the average hybridization.[22,38–40]

Figure 2 shows O K edges acquired by using our spectroscopic equipment. In hematite, as the reported EELS and XAS results,[22,27,41,42] a strong prepeak with a splitting of 1.2 eV can be seen. This prepeak usually decreases with the reduction in iron, which is an evidence of a weaker average hybridization for lower iron valence state as demonstrated in FeO compound[37,41] or $FeCO_3$ compound.[27] In the case of magnetite, several studies have reported an asymmetric O K with a shoulder located a 530 eV on the high-energy side of the prepeak,[24,27] which also can be seen in our spectrum. For maghemite, O K edge is inconsistent from one report to the other. Nevertheless, Paterson[33] and Signorini[43] showed an intense prepeak with an asymmetric splitting where high-energy side peak has a smaller intensity. The splitting is smaller with compared to hematite and has been reported to be around 0.85 eV.[33]

The role of the OH^- bonding plays in the O K edges is still unclear now. Strong prepeak in O K that have been assigned to water exists in minerals[44] at least when transition

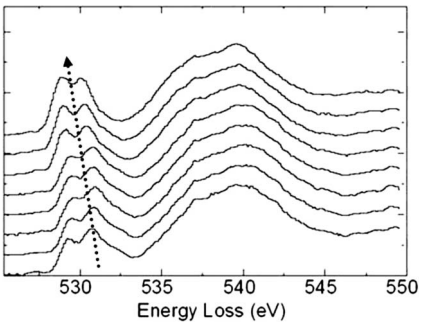

FIG. 3. From bottom to top, time evolution of O *K* edges for reference goethite under the electron beam. The arrow shows the two main effects of the OH removal on the O *K* prepeak: (1) the prepeak moves to lower energy while the last shoulder of the prepeak vanishes, (2) the overall intensity of the prepeak increase as compared to the main edges intensity.

metal are absent.[45] With sufficient energy resolution, several XAS experiments have reported that additional spectral features may be observed in iron hydroxide. O *K* edge in goethite and limonite shows additional features at high-energy side of the prepeak.[27] Similar evolution is also observed by XAS for hydroxide layer on magnetite.[46] In the case of EELS, however, no experimental evidence has been yet reported at the sufficient high-energy resolution, which is necessary to observe the high-energy shoulder of the prepeak of O *K* for iron hydroxide. In Fig. 2, the O *K* edges for the iron hydroxides show a weaker prepeak, usually located at higher energy as compared to the anhydrous phases.

In addition, it has been reported that, with heating or under electron beam, dehydration occurs and the phase transforms from goethite to hematite. So, EELS O *K* edges evolution was measured under the electron beam for a reference goethite sample. The electron beam (200 pA) was focused on an area (~ 1 nm^2) and then one spectrum per 10 s was acquired for eight times (Fig. 3). The initial spectrum is a typical O *K* edge of goethite. There are three subpeaks and shoulder in the prepeak, of which the position was 529, 531, and 532 eV, respectively. With time increasing, some interesting phenomenon was noted. At first, the intensity of prepeak increases remarkably. Next, the peak position of prepeak shifts to lower energy loss region (from 531 to 530.5 eV), and the shoulder located at 532–532.5 eV decreases gradually until it disappears. It can be found that the final spectrum resemble as the O *K* edge of hematite. The above results suggest that a weak prepeak intensity and a shoulder at 532.5 eV may come from the OH^- bonding, as already proposed in Ref. 25. In order to validate this assumption, we have investigated numerically the density of state of hematite, goethite, and partially dehydrated goethite.

IV. CALCULATED O *K* EDGES FOR GOETHITE AND HEMATITE: CHARGE TRANSFER OF IRON-OXYGEN BONDING UNDER DEHYDRATION OF GOETHITE

Figure 4 shows the O *K* for hematite obtained by DFT theory using local spin-density approximation (LSDA) approximation and the so-called LSDA+*U* using an effective on-site coulomb repulsion of 6 eV. In the present figure, the calculations have been done using full-potential augmented plane-wave method.[47,48] All structures have been relaxed using a conjugated gradient. Hematite has a rhombohedra representation with an experimental unit cell at $a=b=c=0.54346$ nm and angles alpha=beta=gamma=55.23° (structural space group is number 161). In order to take into account the antiferromagnetic (AFM) ordering the symmetry has been decreased to the space-group number 148. The AFM ordering along the *c* axis of the conventional hexagonal representation is thus ++−−. The obtained band gap for the LSDA calculation is of 0.6 eV with a magnetic moment per iron atom of around 3.76 Bohr magneton (nonmagnetic calculation gives a metallic ground state). This is in accordance with what is expected for the LSDA approximation where it has been shown that a small gap was obtained for the AFM magnetic solution.[49] The small value of the gap arises from the under estimation of the electronic correlation in this material. An on-site repulsion U_{eff} at around 6 eV has been introduced with $U_{\text{eff}}=U-J$, where *U* is the on-site coulomb repulsion and *J* is the exchange parameter[50] since it gives a band gap of around 2 eV in accordance with the experimental data. The magnetic moment is of around $4.32\mu_B$ slightly under the experimental value (about $5\mu_B$). The DOS (not shown) are in good agreement with the one published for hematite using generalized gradient approximation (GGA) and GGA+*U*.[49] The O *K* edges have been calculated in the dipole approximation with the ground-state electronic properties, further convoluted with a Lorentz and Gaussian function to fit better with the experimental spectrum.[51,52] Despite excitonic/core-hole effects have been neglected, this approximation may sometimes give correct matches with the experimental EELS (Ref. 53) and have been employed in a sake of simplicity. Hematite shows only one type of structural O connected with four neighboring Fe with an average distance of 0.212 nm. Both LSDA and

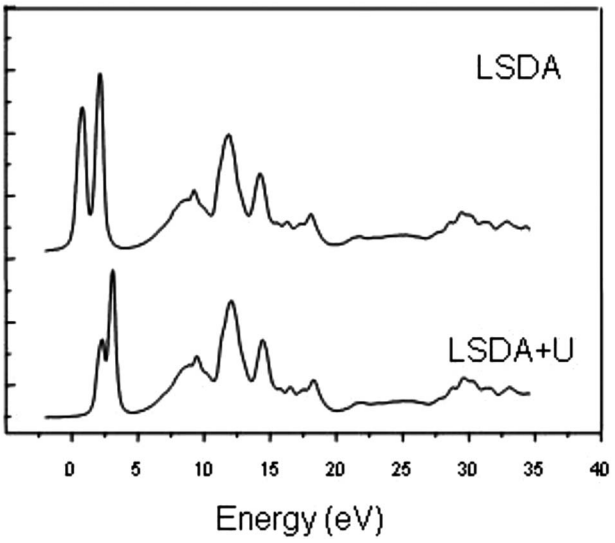

FIG. 4. Calculated O *K* for hematite within LSDA and LSDA+*U* approximation. Energies are expressed from the Fermi level.

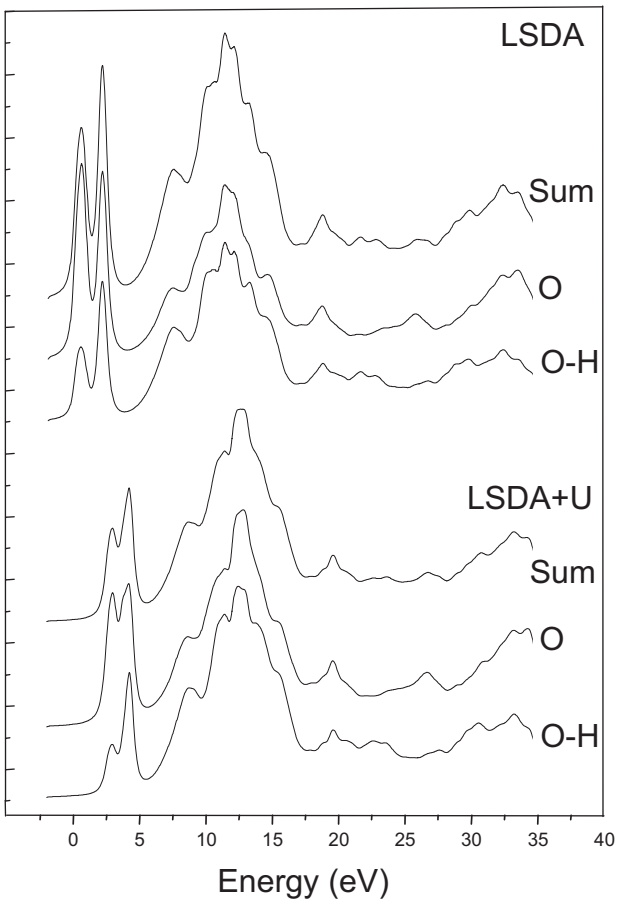

FIG. 5. Calculated O *K* for goethite. LSDA and LSDA+*U* are showed, respectively, in the upper and lower parts. For both parts, the Sum spectra corresponding to the summation over all oxygen in the unit cell is showed. Spectra noted "O" and "O-H" represent, respectively, the spectrum calculated for the oxygen only connected with iron and for the oxygen connected with iron and hydrogen. Energies are expressed from the Fermi level.

LSDA+*U* calculations show a strong prepeak with a visible crystal-field splitting for this oxygen site. As expected the prepeak is shifted toward higher energy for LSDA+*U* calculation where the correct band-gap nature (O 2*p*-Fe 3*d* excitation) and value is obtained. Prepeak splitting is also found smaller for LSDA+*U* at around 1 eV than that for LSDA where a spitting of 1.5 eV is obtained. Both values are comparable to the experimental value of 1.2 eV. On the other hand, the intensity of the first peak is much smaller in the LSDA+*U* calculation than the experimental data revealing that some core-hole effect might anyway not be negligible for these edges.

Similar treatments have been done for the goethite and are shown in Fig. 5. Goethite has an orthorhombic unit cell with a nonmagnetic symmetry corresponding to the space-group number 62. For goethite the magnetic ordering have been set to be +−+− as reported in literature as being the most stable[54] (AFM +−+− magnetic space-group number is 26). Introduction of AFM ordering gives a computed small gap of 0.4 eV with respect to the nonmagnetic solution. Introduction of on-site repulsion of 6 eV gives a gap at the order of 2 eV. In addition of the computed O *K* edges for the whole structure, the spectra obtained for the two structurally nonequivalent oxygen atoms are showed. In goethite an oxygen atom is structural linked to three iron atoms with an average distance of 0.194 nm, while the other is connected to three iron atoms with an average distance of 0.210 nm and one hydrogen atom. Both LSDA and LSDA+*U* reveals that the prepeak of the O *K* edges at the OH bond is much smaller than the other one. The weak intensity of the prepeak is directly an evidence of a weaker hybridization of the Fe and O due to the weaker connectivity and of the presence of an incumbent H. Calculation of the Mulliken population[55,56] confirms that the orbital occupation (O *p*) is higher for the oxygen with the hydrogen (4.94 electrons) compared with the other site (4.84 electrons). On the other hand, we were not able to simulate the third peak (the shoulder at 532.5 eV in the pristine goethite spectrum in Fig. 3) and the projected density of state (neither using full-potential nor pseudopotential techniques) have not indicated that O hybridized with H states were expected at these energy. The experimental measurement of the 523 eV shoulder with the OH is thus believed to account for complex mixture of core-hole effect and correlation effect due to the presence of the H and of a weaker hybridized system.

We have also investigated the influence of the magnetic ordering on the O *K* edges of goethite. Figure 6 shows the O *K* spectra in the case of the stable AFM +−+− ordering and for another AFM ordering where spin align like +−−+ along the *c* direction (in this case the magnetic space group is number 11). Only LSDA calculations are shown in Fig. 6. Taking into account the magnetism symmetry the four oxygen sites in the cell have different symmetry. As a mere example we show in Fig. 6, for both magnetic group, the O *K* edges computed for one oxygen atom from a O-H group. In the +−+− case, the chosen oxygen is connected to one spin-up and two spin-down iron atoms, while in the less stable magnetic group the same structural oxygen is connected to three spin-up iron atoms. Computed spectra show strong difference, noticeably the O *K* line computed for this atomic position in the case of the −++− magnetic ordering has almost no prepeak that arise from the fact that it is connected to iron in the majority spin, thus having only very few density of state in the unoccupied orbitals. Figure 6 also shows the O *K* edges after summation for the oxygen atoms (bonded with or without hydrogen atom) in the different sites. The influence of the magnetic ordering appears smaller. It confirms that the O *K* prepeak intensity is primary sensitive for goethite to the amount of hybridization due to the connectivity or to the presence of H than to the magnetic ordering.

We have finally estimated the formation energy of a hydrogen vacancy in a goethite. Despite formation energy of defects is not directly correlated with the creation rate of defects under the electron beam, they can reveal possible trends on the emissions probabilities.[57,58]

In order to estimate the formation energy of an H vacancy, a supercell containing, respectively, 16, 16, and 32 atoms of Fe, H, and O have been used and a hydrogen atom has been removed. The whole structure have been allowed to structurally relaxed down to a force of 0.01 eV/Å, a maximum displacement of 5.0e-4 Å/atom and a energy difference of

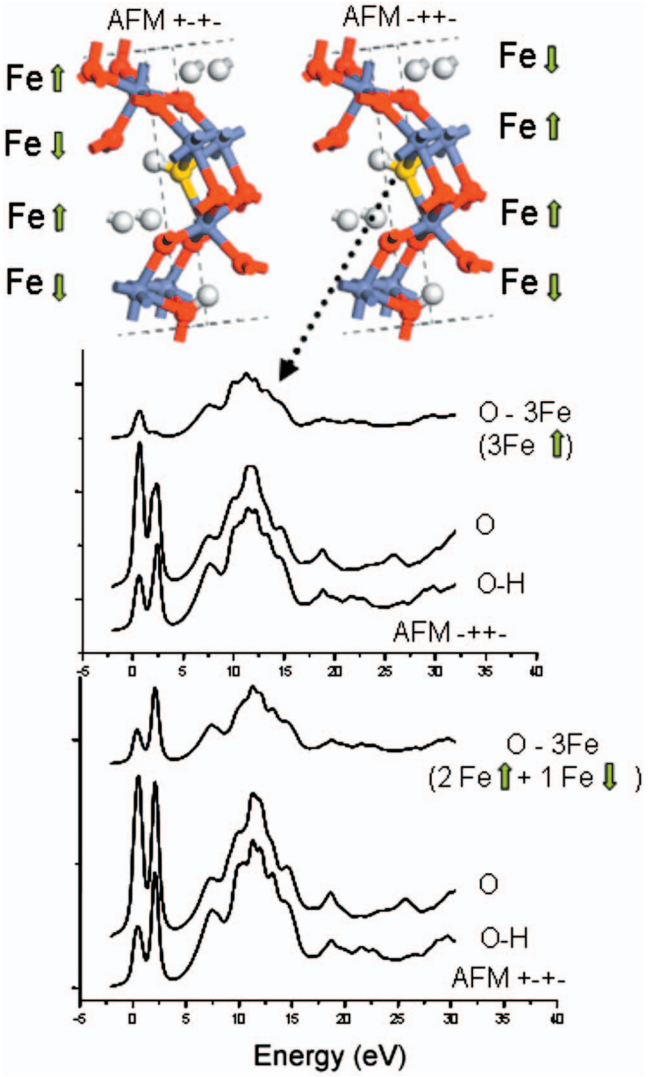

FIG. 6. (Color) Calculated O *K* for goethite for two different magnetic ordering represented in the upper part. Blue, red, and white atoms are iron, oxygen, and hydrogen. Spectra noted "O" and "O-H" represent, respectively, the summed spectrum calculated for the oxygen atoms only connected with iron and for the oxygen atoms connected with iron and hydrogen. At the top of the O and OH spectra, another spectrum calculated for a single atom in the cell (yellow atom in the upper part) but with different magnetic environment is also shown. Energies are expressed from the Fermi level.

5.10e-6 eV/at. The initial magnetic group has been set to be +−+− ordering and has not been constrained during the relaxation (P1 symmetry is used). DFT-LSDA calculation[59] has been obtained using ultrasoft pseudopotential[60] and a nonlinear core correction for the iron.[61] Energy cutoff was 400 eV and a *k*-point meshing corresponding to 0.03 1/Å has been utilized during the relaxation. After structural relaxations, energetic, bands, and orbital populations have been obtained using higher *k* mesh and larger energy cutoff but shows no noticeable difference.

After relaxation, the oxygen where H has been removed, have been suffering the largest displacement. The average distance from this oxygen to the three neighboring Fe atoms

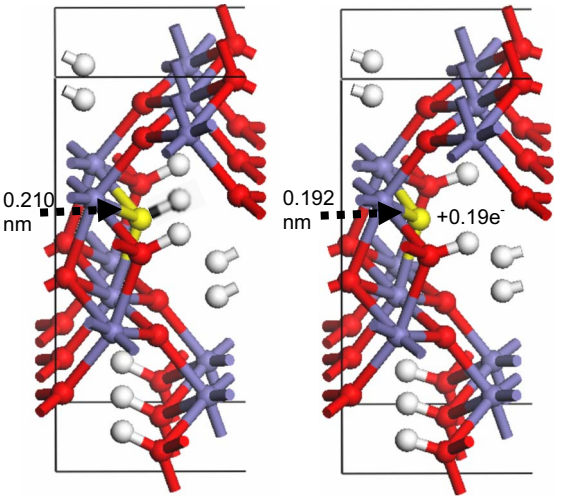

FIG. 7. (Color online) Half-cell representation of the goethite showing the position of the oxygen previously connected to the removed H atom before (left) and after relaxation (right). The removed H atoms is represented shadowed.

decreases from 0.210 to 0.192 nm as shown in Fig. 7. This distance is then compared to the Fe-O bond distance for the non-OH bond of the intact goethite. Other atoms at higher coordination shells show a weak displacement in order to rearrange the structure but without noticeable effect on their electronic or magnetic properties. For example, nonhydroxyl FeO bond located at a distance of 0.5 nm from the defect shows an evolution of its length of less than 0.003 nm. According to this LSDA-based calculation the average spin per iron is about $3.89\mu_B$, which is very comparable to the one of a perfect goethite (LSDA calculation gives $3.97\mu_B$). The removal of single hydrogen from this small supercell (16 irons) and the subsequent contraction of one of the Fe-O clusters do not change the magnetic ordering.

Formation energy of an H vacancy in goethite is estimated of 1.2 eV (taking the H chemical potential for an H_2 dimer), suggesting that both beam heating, knock-on process, and radiolysis may easily be responsible for the dehydration of goethite under the electron beam. Furthermore, projected density of state and orbital populations have confirmed that after H removal and further relaxation, the O previously connected to the hydrogen has a much higher hybridization with the neighboring iron atoms. Indeed, around 0.19 electrons have been back transferred from the oxygen *p* orbitals to primary the iron *d* orbitals during the relaxation, as estimated by Mulliken charge analysis.

This confirms why under electron beam the goethite spectra evolve rapidly toward the spectra of a hematitelike material, i.e., a more intense prepeak and a disappearance of the high-energy shoulder of this prepeak.

V. ANALYSIS OF IRON-OXYGEN NANOMATERIALS GROWN BY HYDROTHERMAL PROCESS

The above experimental and calculated results implicate that EELS can be used to identify iron oxide or hydroxide with various valence and structure. Here we utilize the tech-

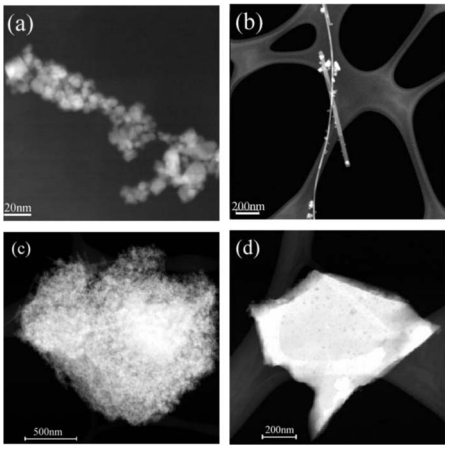

FIG. 8. STEM/HAADF results of (a) agglomerate of magnetite raw nanoparticles (NP) used for the hydrothermal process; (b) 40 h, both long twisted wire and short straight wire are visible. They might be covered partially with particles. Agglomerate of NP can also be detected (not shown); [(c) and (d)] 60 h, only shorter wires are detected (not shown), large cluster of NP are still visible, and large platelet have appeared.

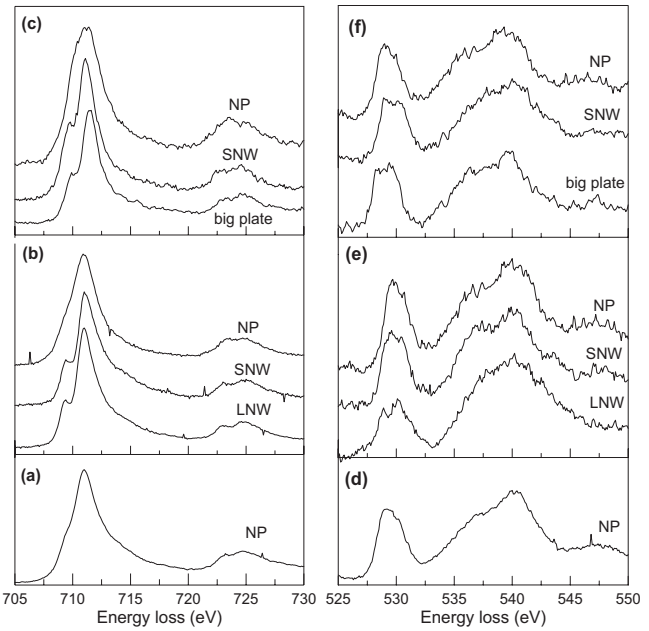

FIG. 9. Electron energy loss spectra obtained from different parts of iron-oxygen compounds. Left figure is Fe *L* edge and right figure is O *K* edge. (a) and (d) are raw particle, (b) and (e) are 40 h, (c) and (f) are 60 h.

nique on an iron-oxygen nanomaterials system prepared by hydrothermal process. Figure 8 shows the STEM/HAADF results of raw particles and products with different reaction time. The size of the raw particles ranges from 10 to 40 nm. After 40 h of reaction time, except for particles, two types of nanowires were obtained. One is long and twisted along the long axis while the other is short and straight. The length of wires ranges from few tens of nanometer to several micrometer. With longer reaction time (60 h), long wires disappeared. More particularly, addition to the clusters of nanoparticles and short nanowires, a lot of platelets in large size (around several microns) were found in this sample.

According to the STEM/HAADF results, it is expected that there are more than one phase existing in the sample. EELS was then performed to identify the phase. The results are described as follows.

A. Raw particle

Fe *L* edge of the raw particles are shown in Fig. 9(a). Two evident peaks ($L_{2,3}$) were observed. L_3 edge is unsymmetrical. It locates at 711 eV with a shoulder at 709.5 eV. L_2 edge is composed of two distinct peaks, in which the peak at high energy (725 eV) is stronger than the other one (723.5 eV). O *K* of the raw particles is shown in Fig. 9(d). The maximum line of prepeak is at around 529 eV with a shoulder at higher energy. Above results of Fe $L_{2,3}$ and O *K* indicate that raw particles are magnetite or magnetite with slight contribution of an oxidized surface. It is coincident with the SAED analysis of cluster of particles which show a spinel structured powder diffraction.

B. 40 h

After 40 h reaction, particles, short nanowires (SNW) and long nanowires (LNW) are detected. Electron diffraction results confirm that the particles are spinel structure. Fe *L* and O *K* for particles are the same as those of raw particles. These results indicate that particles are magnetite. From the EELS spectra presented in Fig. 9(b), the fine structure of NP is completely similar to the reference magnetite. But small oxidation traces have also been detected on some NPs. As for the wires, in Fe *L* edge, there is no difference between SNW and LNW, as shown in Fig. 9(b). The splitting of L_3 is about 1.3 eV. In L_2 edge, the relative height of the two peaks is inversely with comparing to raw particles. The above Fe *L* edge demonstrates iron is ferric for both SNW and LNW with a rather small crystal-field splitting (compatible with maghemite or hydroxide but not with hematite or magnetite). From Fig. 9(e), it can be seen that O *K* in SNW is similar to that of particles (at least they show a strong prepeak with a large shoulder in the higher-energy side that is certainly the evidence of an anhydrous iron oxide such as maghemite). In LNW, a smaller prepeak (with various fine structures including the high-energy bump reported as an contribution to the OH-in the structure as mentioned before) is visible. Under the beam, the prepeak of the O *K* of LNW increased in a similar way as reported in Fig. 3. Accordingly, in 40 h sample, we believed that SNW is maghemite and LNW is goethite. This is confirmed by SAED diffraction pattern obtained on oriented single wire (for example, [110] zone axis of spinel structures have been observed for SNW and [101] zone axis of goethite have been observed for LNW).

C. 60 h

After 60 h reaction, as mentioned before, there are many aggregations which were composed of SNW and particles.

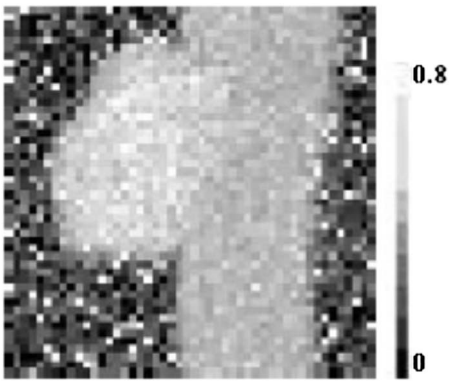

FIG. 10. EELS chemical mapping results of the nanoparticle and nanowire. The ratio between Fe and O (Fe/O) of the particle is about 0.75, which is the same with Fe_3O_4. For the wire, the ratio ranges from 0.55 to 0.65, which is comparable with a FeOOH compound that had partially transforms to Fe_2O_3 (beam induced dehydration). Image size of 80×80 nm.

As shown in Figs. 9(c) and 9(f), both the Fe *L* and O *K* edges in the particles are similar to that of particles in 40 h sample. As for SNW, however, both the peak locates at 709.7 eV in Fe L_3 edge and the shoulder at 530 eV in the O *K* are larger than those in 40 h sample. Based on the abovementioned ELNES, these results imply that with longer reaction time, NW and particle will contain more water and the iron will reduce. As for the big platelet, Fe *L* edge shows trivalent iron, as shown in Fig. 9(c). Two distinct peaks with equivalent height were observed in the prepeak of O *K* [Fig. 9(f)]. The splitting between these two peaks is 1.2 eV. The above results indicate that the large platelets are hematite and this tally with diffraction results. Indeed, hematite is a common end product for aging iron oxide solution.

Quantitative elemental measurements were also performed. The Fe/O ratio was obtained according to the equation, $\mathrm{Fe/O} = I(\mathrm{Fe}) \times I(\mathrm{O}) / \sigma\mathrm{O} \times \sigma\mathrm{Fe}$, where σ is the cross section (computed within a hydrogenic model with white line correction or within an Hattre-Slater approximation) and I is the intensity of the subtracted edge. In this study, the energy range for the edges integration is 80 eV. Figure 10 shows the results of Fe/O ratio mapped onto an area of 80 by 80 nm including a particle and a wire. An EELS spectrum have been collected on every position of the 48×48 image with an acquisition time of 50 ms. The ratio ranges from 0.75–0.76 for the particles and it ranges from 0.55 to 0.65 for the wires. This is coincident with above phase identifications, which imply particles are Fe_3O_4 and wires are Fe_2O_3 or FeOOH. These values were also comparable to the results of Colliex *et al.*[10] Notably, it is found that in the particle, the Fe/O value in the surface is lower (darker contrast) than that inside and that in the surface of NW, some bright contrast are seen, indicating that the Fe/O ratio there is larger. This con-

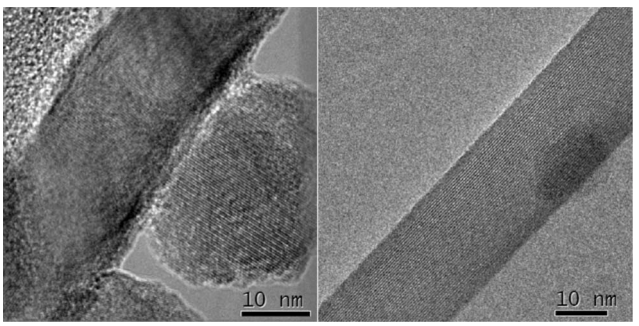

FIG. 11. 40 h sample, HRTEM results for NP particle and of LNW wire. (Left) NPs have rough and irregular surfaces where crystallization are not observed; (right) LNW goethite nanorod.

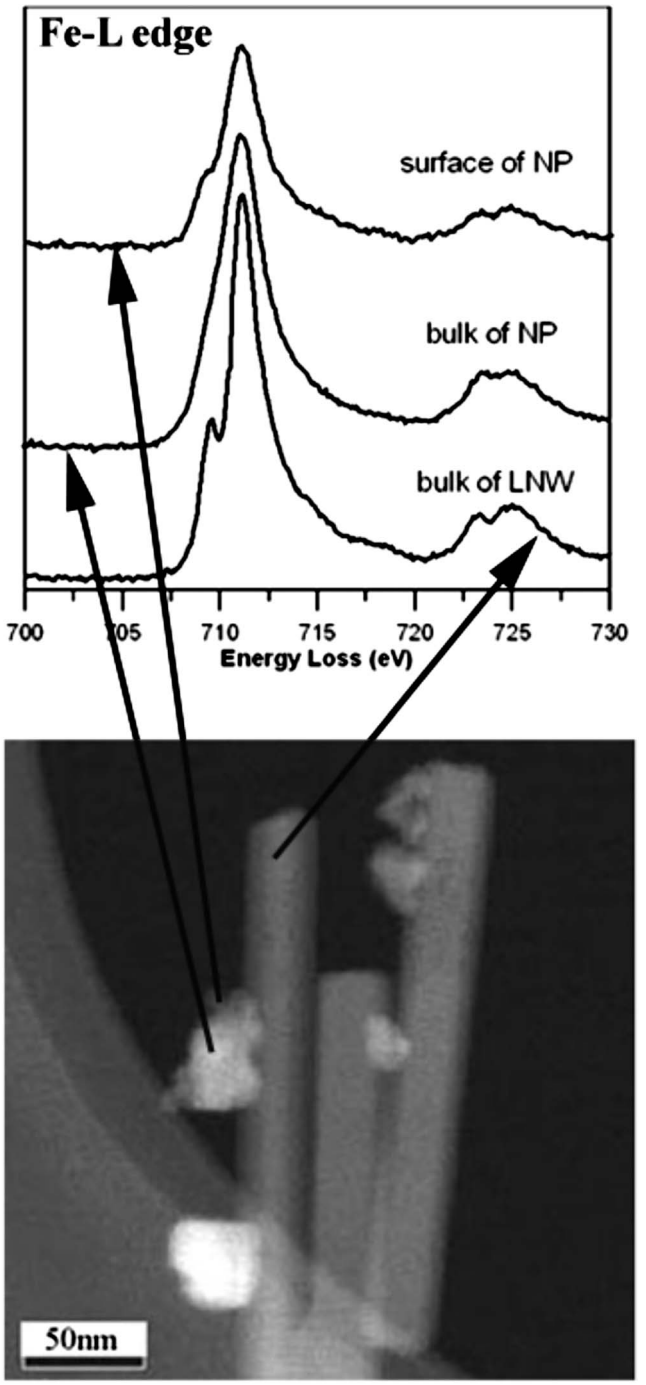

FIG. 12. 40hrs sample, Fe *L* edge obtained from particles, the surface of a particles and LNW. While bulk NP shows a Fe *L* edges very similar to a magnetite, its surface spectrum shows some trivalent iron. LNW has a Fe^{3+} EELS signature.

firms that the surface of the magnetite NP can be oxidized and that the NW structure can be partially reduced at the surface (electron damage for this high spatially resolved experiment might be one of the causes). HRTEM observations found a rough surface for the NP corresponding to a thin amorphous layer on their surfaces. As shown in Fig. 11, the thickness of the amorphous layer is about 3 nm and it may correspond to the oxidized section of the magnetite. On the other hand, the surface of the "intact" LNW made of goethite do not show amorphous layer. But such layer appears with longer acquisition time (not shown in the figure). We thus believed that the amorphous layer in the NP is due to the alteration, oxidation, or precipitation-reprecipitation process in the hydrothermal treatment but that the amorphous layer in LNW are only electron-beam artifact.

Spatially resolved EELS fine-structure analysis was then carried out to study the difference of electronic structure between surface and inside. Figure 12 confirms that the Fe L edges at the surface of the magnetite NP had a weak splitting of the L_3 line and a nonmagnetitelike L_2 edge which is an evidence of a small oxidation.

The EELS, STEM, SAED, and HREM nanoanalyses of the iron oxides obtained by hydrothermal treatment of magnetite nanoparticles reveal a complex system. Up to four different phases among the iron-oxygen compounds are observed: some of the nanowires (NW) are maghemite (γ-Fe_2O_3) phase and others are goethite (α-FeOOH). The nanoparticles (NP) observed in the product are magnetite (Fe_3O_4) with the surface altered during the hydrothermal process. After long reaction time, α-Fe_2O_3 in the form of large platelet was found. In addition, iron valence can change on a nanometer scale due to surface oxidation or can be reduced under the electron beam. Dehydration is also observed under the electron irradiation.

VI. CONCLUSION

Reference experiments (at the Fe $2p$ and O $1s$ edges) and *ab initio* calculations showed how electron energy loss spectroscopy (EELS) can be used in order to characterize phases of iron oxide/hydroxide nanomaterials. In particular, we show that dehydration of iron hydroxide such as goethite can easily appear under the electron beam but might be followed by monitoring the O K peak. Indeed, both LSDA and LSDA+U calculations confirm that intensity of the prepeak of the O K should increase while H atoms are removed, either under the heating or knock-on effect from the electron beam.

According to the quantitative elemental measurements and ELNES, we have been able to report the complexity of nanowires and nanoparticles obtained under hydrothermal treatment, and we have identified up to four different phases among the iron-oxygen compounds: some of the nanowires are maghemite (γ-Fe_2O_3) phase and others are goethite (α-FeOOH). The nanoparticles observed in the product are magnetite (Fe_3O_4) and the big platelets in the final are hematite (α-Fe_2O_3). The surface of particles altered during the hydrothermal process. This show how cautious physical properties such as magnetic measurement on such system should be interpreted with care and in close relation of the structural investigation of the product. Noticeably, this study also demonstrated that the combination of ED (electron diffraction), HREM, and EELS at high-energy resolution is a powerful tool to study the TM (transition metal) valence in nanoscale materials.

ACKNOWLEDGMENTS

This research is supported by the National Science Council of Taiwan, Republic of China, under the Contract No. NSC 96-2112-M-011-004-MY2.

*Corresponding author. SYChen@mail.ntust.edu.tw
†Corresponding author. gloter@lps.u-psud.fr

[1] J. Wang, Q. Chen, C. Zeng, and B. Hou, Adv. Mater. **16**, 137 (2004).
[2] S. Lian, E. Wang, L. Gao, Z. Kang, D. Wu, Y. Lan, and L. Xu, Solid State Commun. **132**, 375 (2004).
[3] J. Park, K. An, Y. Hwang, J. G. Park, H. J. Noh, J. Y. Kim, J. H. Park, N. M. Hwang, and T. Hyeon, Nat. Mater. **3**, 891 (2004).
[4] C. R. Brundle, T. J. Chuang, and K. Wendelt, Surf. Sci. **68**, 459 (1977).
[5] R. D. Leapman, L. A. Grunes, and P. L. Fejes, Phys. Rev. B **26**, 614 (1982).
[6] J. Fink, T. Muller-Heinzerling, B. Scheerer, W. Speier, F. U. Hillebrecht, J. C. Fuggle, J. Zaanen, and G. A. Sawatzky, Phys. Rev. B **32**, 4899 (1985).
[7] R. D. Leapman and L. A. Grunes, Phys. Rev. Lett. **45**, 397 (1980).
[8] R. Vijaya Kumar, Y. Koltypin, X. N. Xu, Y. Yeshurun, A. Gedanken, and I. Felner, J. Appl. Phys. **89**, 6324 (2001).
[9] S. Lian, E. Wang, L. Gao, Z. Kang, D. Wu, Y. Lan, and L. Xu, Solid State Commun. **132**, 375 (2004).
[10] C. Colliex, T. Manoubi, and C. Ortiz, Phys. Rev. B **44**, 11402 (1991).
[11] L. A. J. Garvie, T. J. Zega, P. Rez, and P. R. Buseck, Am. Mineral. **89**, 1610 (2004).
[12] L. A. J. Garvie and P. R. Buseck, Nature (London) **396**, 667 (1998).
[13] P. A. van Aken, B. Liebscher, and V. J. Styrsa, Phys. Chem. Miner. **25**, 323 (1998).
[14] P. A. van Aken and B. Liebscher, Phys. Chem. Miner. **29**, 188 (2002).
[15] J. P. Crocombette, M. Pollak, F. Jollet, N. Thromat, and M. Gautier-Soyer, Phys. Rev. B **52**, 3143 (1995).
[16] P. Kuiper, B. G. Searle, P. Rudolf, L. H. Tjeng, and C. T. Chen, Phys. Rev. Lett. **70**, 1549 (1993).
[17] I. Letard, Ph. Sainctavit, N. Menguy, J. P. Valet, A. Isambert, M. Dekkers, and A. Gloter, Phys. Scr. **T115**, 489 (2005).
[18] A. Gloter, M. Zbinden, F. Guyot, F. Gaill, and C. Colliex, Earth Planet. Sci. Lett. **222**, 947 (2004).
[19] J. J. Dynes, T. Tyliszczak, T. Araki, J. R. Lawrence, G. D. W.

Swerhone, G. G. Leppard, and A. P. Hitchcock, Environ. Sci. Technol. **40**, 1556 (2006).
[20] G. van der Laan and I. W. Kirkman, J. Phys.: Condens. Matter **4**, 4189 (1992).
[21] J. Tafto and O. L. Krivanek, Phys. Rev. Lett. **48**, 560 (1982).
[22] A. Gloter, J. Ingrin, D. Bouchet, and C. Colliex, Phys. Rev. B **61**, 2587 (2000).
[23] P. A. van Aken and S. Lauterbach, Phys. Chem. Miner. **30**, 469 (2003).
[24] A. Gloter, A. Douiri, M. Tence, and C. Colliex, Ultramicroscopy **96**, 385 (2003).
[25] L. Stichauer, A. Mirone, S. Turchini, T. Prosperi, S. Zennaro, N. Zema, F. Lama, R. Pontin, Z. Simsa, Ph. Tailhades, and C. Bonningue, J. Appl. Phys. **90**, 2511 (2001).
[26] M. Sacchi, C. F. Hague, S. Gota, E. Guiot, M. Gautier-Soyer, L. Pasquali, S. Mrowka, E. M. Gullkson, and J. H. Underwood, J. Electron Spectrosc. Relat. Phenom. **101–103**, 407 (1999).
[27] T. Kendelewicz, P. Liu, C. S. Doyle, G. E. Brown, Jr., E. J. Nelson, and S. A. Chambers, Surf. Sci. **453**, 32 (2000).
[28] P. Kuiper, B. G. Searle, L. C. Duda, R. M. Wolf, and P. J. Van der Zaag, J. Electron Spectrosc. Relat. Phenom. **86**, 107 (1997).
[29] C. L. Chen, G. Chern, W. L. Pan, P. K. Tseng, and C. L. Chang, J. Electron Spectrosc. Relat. Phenom. **144–147**, 921 (2005).
[30] C. L. Chang, G. Chern, C. L. Chen, H. H. Hsieh, C. L. Dong, W. F. Pong, C. H. Chao, H. C. Chien, and S. L. Chang, Solid State Commun. **109**, 599 (1999).
[31] J. Chen, D. J. Huang, A. Tanaka, C. F. Chang, S. C. Chung, W. B. Wu, and C. T. Chen, Phys. Rev. B **69**, 085107 (2004).
[32] T. Fujii, F. M. F. de Groot, G. A. Sawatzky, F. C. Voogt, T. Hibma, and K. Okada, Phys. Rev. B **59**, 3195 (1999).
[33] C. S. Chan, G. De Stasio, S. A. Welch, M. Girasole, B. H. Frazer, M. V. Nesterova, S. Frarka, and J. F. Banfield, Science **303**, 1656 (2004).
[34] A. D. Smith, G. Cressey, P. F. Schofield, and B. A. Cressey, J. Synchrotron Radiat. **5**, 1108 (1998).
[35] E. Pellegrain, M. Hagelstein, S. Doyle, H. O. Moser, J. Fuchs, D. Vollath, S. Schuppler, M. A. James, S. S. Saxena, L. Niesen, O. Rogojanu, G. A. Sawatzky, C. Ferrero, M. Borowski, O. Tjernberg, and N. B. Brookes, Phys. Status Solidi B **215**, 797 (1999).
[36] J. H. Paterson, Ultramicroscopy **32**, 319 (1990).
[37] S. Brice-Profeta, M. A. Arrio, E. Tronc, N. Menguy, I. Letard, C. C. D. Moulin, M. Nogues, C. Chaneac, J. P. Jolivet, and P. Sainctavit, J. Magn. Magn. Mater. **288**, 354 (2005).
[38] F. M. F. de Groot, M. Grioni, J. C. Fuggle, J. Ghijsen, G. A. Sawatzky, and H. Petersen, Phys. Rev. B **40**, 5715 (1989).
[39] Z. Hu, M. S. Golden, J. Fink, G. Kaindl, S. A. Warda, D. Reinen, Priya Mahadevan, and D. D. Sarma, Phys. Rev. B **61**, 3739 (2000).
[40] Z. Hu, Chandan Mazumdar, G. Kaindl, F. M. F. de Groot, S. A. Warda, and D. Reinen, Chem. Phys. Lett. **297**, 321 (1998).
[41] C. Mitterbauer, G. Kothleitner, W. Grogger, H. Zandbergen, B. Freitag, P. Tiemeijer, and F. Hofer, Ultramicroscopy **96**, 469 (2003).
[42] M. K. Wu, J. R. Ashburn, C. J. Torng, P. H. Hor, R. L. Meng, L. Gao, Z. J. Huang, Y. Q. Wang, and C. W. Chu, Phys. Rev. Lett. **58**, 908 (1987).
[43] L. Signorini, L. Pasquini, L. Savini, R. Carboni, F. Boscherini, E. Bonetti, A. Giglia, M. Pedio, N. Mahne, and S. Nannarone, Phys. Rev. B **68**, 195423 (2003).
[44] R. Wirth, Phys. Chem. Miner. **24**, 561 (1997).
[45] P. A. van Aken, B. Liebscher, and V. J. Styrsa, Phys. Chem. Miner. **25**, 494 (1998).
[46] T. Kendelewicz, P. Liu, C. S. Doyle, G. E. Brown, Jr., and S. A. Chambers, Surf. Sci. **424**, 219 (1999).
[47] P. Blaha, K. Schwarz, G. K. H. Madsen, D. Kvasnicka, and J. Luitz, WIEN2K, 2001.
[48] P. Blaha, K. Schwarz, P. Sorantin, and S. B. Trickey, Comput. Phys. Commun. **59**, 399 (1990).
[49] G. Rollmann, A. Rohrbach, P. Entel, and J. Hafner, Phys. Rev. B **69**, 165107 (2004).
[50] V. I. Anisimov, I. V. Solovyev, M. A. Korotin, M. T. Czyzyk, and G. A. Sawatzky, Phys. Rev. B **48**, 16929 (1993).
[51] K. Schwarz, and E. Wimmer, J. Phys. F: Met. Phys. **10**, 1001 (1980).
[52] K. Schwarz and P. Blaha, Lect. Notes Chem. **67**, 139 (1996).
[53] G. Radtke, Ultramicroscopy **108**, 893 (2008).
[54] J. M. D. Coey, A. Barry, J. Brotto, H. Rakoto, S. Brennan, W. N. Mussel, A. Collomb, and D. Fruchart, J. Phys.: Condens. Matter **7**, 759 (1995).
[55] M. D. Segall, C. J. Pickard, R. Shah, and M. C. Payne, Mol. Phys. **89**, 571 (1996).
[56] M. D. Segall, R. Shah, C. J. Pickard, and M. C. Payne, Phys. Rev. B **54**, 16317 (1996).
[57] A. Zobelli, C. Ewels, A. Gloter, G. Seifert, O. Stephan, S. Csillag, and C. Colliex, Nano Lett. **6**, 1955 (2006).
[58] A. Zobelli, A. Gloter, C. P. Ewels, G. Seifert, and C. Colliex, Phys. Rev. B **75**, 245402 (2007).
[59] M. D. Segall, P. J. D. Lindan, M. J. Probert, C. J. Pickard, P. J. Hasnip, S. J. Clark, and M. C. Payne, J. Phys.: Condens. Matter **14**, 2717 (2002).
[60] D. Vanderbilt, Phys. Rev. B **41**, 7892 (1990).
[61] S. G. Louie, S. Froyen, and M. L. Cohen, Phys. Rev. B **26**, 1738 (1982).